

---

---

# Clinical Validation of $^{18}\text{F}$ -AZD4694, an Amyloid- $\beta$ -Specific PET Radioligand

Zsolt Cselényi<sup>1,2</sup>, Maria Eriksson Jönhagen<sup>3,4</sup>, Anton Forsberg<sup>2</sup>, Christer Halldin<sup>2</sup>, Per Julin<sup>1</sup>, Magnus Schou<sup>1,2</sup>, Peter Johnström<sup>1,2</sup>, Katarina Varnäs<sup>2</sup>, Samuel Svensson<sup>1</sup>, and Lars Farde<sup>1,2</sup>

<sup>1</sup>Neuroscience Research and Therapy Area, AstraZeneca Research and Development, Södertälje, Sweden; <sup>2</sup>Centre for Psychiatry Research, Department of Clinical Neuroscience, Karolinska Institutet, Stockholm, Sweden; <sup>3</sup>Clinical Geriatrics, Department of Neurobiology, Caring Sciences and Society, Karolinska Institutet, Stockholm, Sweden; and <sup>4</sup>Department of Geriatric Medicine, Karolinska University Hospital, Stockholm, Sweden

---

Pioneered with the invention of  $^{11}\text{C}$ -Pittsburgh compound B, amyloid- $\beta$  imaging using PET has facilitated research in Alzheimer disease (AD). This imaging approach has promise for diagnostic purposes and evaluation of disease-modifying therapies. Broad clinical use requires an  $^{18}\text{F}$ -labeled amyloid- $\beta$  radioligand with high specific and low nonspecific binding. The aim of the present PET study was to examine the radioligand  $^{18}\text{F}$ -AZD4694 in human subjects. **Methods:** Six control subjects and 10 clinically diagnosed AD patients underwent PET examination with  $^{18}\text{F}$ -AZD4694 and a structural MRI scan. Of these, 4 controls and 4 patients underwent a second PET examination for test-retest analysis. Arterial sampling was done to derive a metabolite-corrected plasma input function for traditional compartment modeling. Besides, several simplified quantitative approaches were applied, including the reference Logan approach and simple ratio methods. **Results:** After intravenous injection of  $^{18}\text{F}$ -AZD4694, radioactivity appeared rapidly in brain. In patients, radioactivity was high in regions expected to contain amyloid- $\beta$ , whereas in controls, radioactivity was low and homogeneously distributed. Binding in cerebellum, a reference region, was low and similar between the groups. Specific binding was reversible and peaked at about 27 min after injection in regions with high radioactivity. The time-activity curves could be described using the 2-tissue-compartment model. Distribution volume ratio estimates obtained using compartment models and simplified methods were highly correlated. Standardized uptake value ratios calculated at late times and distribution volume ratios estimated with the reference Logan approach were, in gray matter, significantly lower in control subjects (1.08 [11%] and 1.01 [6%], respectively) than in AD patients (2.15 [24%] and 1.62 [18%], respectively). Among non-invasive methods, the lowest test-retest variability was found with reference Logan, varying between 4% and 6% across brain regions. **Conclusion:** Noninvasive quantitative approaches provide valid estimates of amyloid- $\beta$  binding. Because of the radioisotope ( $^{18}\text{F}$ ) used for labeling, the radioligand has potential for wide clinical application.  $^{18}\text{F}$ -AZD4694 satisfies the requirements for a promising amyloid- $\beta$  radioligand both for diagnostic use and for evaluation of disease-modifying therapies in AD.

**Key Words:** PET; amyloid-beta; radioligand;  $^{18}\text{F}$ ; Alzheimer's disease

**J Nucl Med 2012; 53:415–424**

DOI: 10.2967/jnumed.111.094029

---

**A**lzheimer disease (AD) was identified more than a century ago on the basis of histopathologic observations. The diagnosis of AD, however, is a clinical challenge, and a definite diagnosis can still only be made after death. In clinical research on AD, the search for sensitive and specific in vivo biomarkers has thus been given high priority. A promising recent approach is the use of PET and radiolabeled ligands targeting amyloid- $\beta$  deposits in the brain. The first and so far most successful radioligand is  $^{11}\text{C}$ -labeled 2-[4'-(methylamino)phenyl]-6-hydroxybenzothiazole ( $^{11}\text{C}$ -PIB), which binds predominantly to amyloid- $\beta$  plaques in the human brain (1). Initial studies have shown that control subjects (CSs) and AD patients can be separated on the basis of their amyloid- $\beta$  load (2). Subsequently, in vivo amyloid- $\beta$  imaging has been applied in research on early AD diagnosis (3), evaluation of longitudinal progression of disease (4), and evaluation of new disease-modifying therapies (5).

This first generation of amyloid- $\beta$  radioligands has thereby opened a new field of neuroimaging research. Radioligands such as  $^{11}\text{C}$ -PIB have affinity for amyloid- $\beta$  in the low-nanomolar range, and a favorable near-stable signal-to-background ratio is obtained during the later phase of data acquisition (6). By consequence, a late-time-ratio approach often referred to as a quasi-steady-state approach has routinely been applied to obtain quantitative measures (7).

Traditional development of radioligands used for neuroreceptor imaging has followed a different path. Radioligands such as  $^{11}\text{C}$ -raclopride (8) have routinely been examined using compartment analysis with a metabolite-corrected arterial input function (8). The compartment analysis has then been used to validate simplified reference region approaches for calculation of binding potential.

---

Received Jun. 1, 2011; revision accepted Oct. 25, 2011.  
For correspondence or reprints contact: Zsolt Cselényi, Clinical Development, Early Development NS, B230, Kvambergagatan 12, Södertälje, Sweden, S-151 85.  
E-mail: zsold.cselenyi@astrazeneca.com  
Published online Feb. 9, 2012.  
COPYRIGHT © 2012 by the Society of Nuclear Medicine, Inc.

Whereas  $^{11}\text{C}$ -labeled radioligands have a half-life of 20 min,  $^{18}\text{F}$ -labeled radioligands have the advantage of a longer half-life (110 min), making it possible to ship to PET centers without a cyclotron. In recent years, several  $^{18}\text{F}$ -labeled compounds have been developed and examined in vivo (9–11), but only  $^{18}\text{F}$ -flutemetamol has so far been described in detail in the literature using a compartment analysis with arterial input function (12).

A new benzofuran radioligand,  $^{18}\text{F}$ -AZD4694, has been developed in a collaboration between Karolinska Institutet and AstraZeneca and characterized in preclinical assays (13).  $^{18}\text{F}$ -AZD4694 has high affinity to amyloid- $\beta$  fibrils in vitro ( $K_d$ ,  $2.3 \pm 0.3$  nM) and shows selective labeling of amyloid- $\beta$  in cortical sections from postmortem human AD brains.

The aim of the present PET study was to examine in detail the binding of  $^{18}\text{F}$ -AZD4694 to amyloid- $\beta$  in 6 CSs and 10 patients with AD.  $^{18}\text{F}$ -AZD4694 binding was examined using compartment analysis with a metabolite-corrected arterial input function and reference region-based quantitative approaches. In addition, 8 of the enrolled subjects (4 CSs and 4 AD patients) were reexamined to obtain a preliminary estimate of test-retest reproducibility.

## MATERIALS AND METHODS

### Subjects and Study Design

The study was approved by the Regional Ethics Committee in Stockholm and was performed in accordance with the Declaration of Helsinki and the guidelines of the International Conference on Harmonization/Good Clinical Practice. All subjects and caregivers gave written informed consent before enrollment in the study.

Six CSs and 10 patients with AD were included. The patients were recruited from the Memory Clinic at Karolinska University Hospital Huddinge, Sweden. AD was diagnosed according to the DSM-IV criteria of dementia (14). The patient characterization included patient and informant interview, neurologic examination, Mini-Mental State Examination, psychometric testing of cognition, and brain imaging (MRI or CT). On the basis of this information, a team conference established the clinical diagnosis. The inclusion criteria included age between 50 and 80 y, Mini-Mental State Examination scores of 16–26, and weight between 55 and 100 kg. The main exclusion criterion was significant cerebrovascular or other somatic disease apart from AD.

CSs were considered healthy after undergoing a thorough clinical examination including blood and urine analysis and on exhibiting a Mini-Mental State Examination score of greater than 28.

All subjects participated in 1 PET examination with  $^{18}\text{F}$ -AZD4694. To examine the test-retest variability of  $^{18}\text{F}$ -AZD4694, 4 CSs and 4 AD patients underwent a second PET examination after 7–20 d.

### MRI and PET Experimental Procedure

All subjects underwent MRI on a 1.5-T Avanto scanner (Siemens) at Karolinska University Hospital. T1-weighted MR images were obtained for each individual and used for gray and white matter segmentation and delineation of regions of interest (ROIs). The 3-dimensional MRI dataset was reoriented so that the line between the anterior and posterior commissures was on the horizontal plane and the interhemispheric fissure was on the sagittal

plane. The MR image was segmented into gray matter, white matter, and cerebrospinal fluid segments using the SPM5 segmentation algorithm (Wellcome Trust Centre for Neuroimaging) in MATLAB (The MathWorks Inc.).

$^{18}\text{F}$ -AZD4694 was prepared by radiofluorination of its corresponding *N*-Boc-protected nitro precursor followed by acidic deprotection (as described in patent WO20100056796).  $^{18}\text{F}$ -AZD4694 was obtained in a 6% overall radiochemical yield (corrected for decay) with a specific radioactivity between 16 and 290 GBq/ $\mu\text{mol}$  at the time of intravenous bolus administration.  $^{18}\text{F}$ -AZD4694 was injected as a bolus with a mean radioactivity of  $203 \pm 6$  MBq (range, 194–218 MBq). There were no significant differences in injected radioactivity and specific radioactivity between CSs and AD patients ( $P > 0.05$ ).

PET data were obtained with a high-resolution research tomograph (HRRT; Siemens/CTI) operating in list mode (15). Data were acquired for 93 min after intravenous injection. The list-mode data were binned and reconstructed using iterative reconstruction with point-spread function modeling into a 4-dimensional PET image containing 38 consecutive time frames ( $9 \times 10$  s,  $2 \times 15$  s,  $3 \times 20$  s,  $4 \times 30$  s,  $4 \times 60$  s,  $4 \times 180$  s and  $12 \times 360$  s) with a 3-dimensional array of  $256 \times 256 \times 207$  voxels having a size of  $1.22 \times 1.22 \times 1.22$  mm (15).

### Arterial Input Function

Continuous arterial sampling was performed during the initial 10 min using an automated blood sampling system to derive a metabolite-corrected plasma input function, as described before (8). Discrete manual arterial samples were drawn at scheduled time points during the PET examination (4, 10, 20, 30, 40, 50, 60, 70, 80, and 90 min) for measurement of whole-blood and plasma radioactivity concentration. The analysis of radioligand metabolites was performed using standard methodology as described previously (16).

### ROIs

Anatomic ROIs were manually delineated on the reoriented,  $1 \times 1 \times 1$  mm resolution MR image using the human brain atlas (17). ROIs were delineated as regions previously described (18) for the anterior cingulate cortex, lateral temporal cortex, parietal cortex, posterior cingulate cortex, prefrontal cortex, and cerebellum. Segmented images of total gray matter, white matter, and whole brain (defined as gray matter plus white matter) were created during image processing and used to generate the respective ROIs. When the manually delineated cortical ROIs were applied to the PET image, the gray matter segment was used to include only gray matter voxels.

### Quantitative Analyses

Detailed descriptions of the quantitative approaches are given in the supplemental data (supplemental materials are available online only at <http://jnm.snmjournals.org>). Initially, the binding of  $^{18}\text{F}$ -AZD4694 was interpreted using the 1-tissue-compartment model and the 2-tissue-compartment model with a metabolite-corrected arterial input function (8). Subsequently, simplified methods with or without the use of a reference region were examined for cross-validation purposes (19).

Two linear graphical methods proposed by Logan et al. were applied (20). First, using the metabolite-corrected arterial blood curve as input function, the last 10 points of the Logan plot were fitted to obtain the total distribution volume (33–93 min after injection). Second, using the cerebellum as reference region (reference Logan), the last 11 points of the linear plot were fitted to

obtain distribution volume ratio (DVR) (27–93 min after injection) (21). The reference Logan approach was further examined with regard to the measurement time, with alternate start time or end time used to fit the regression line on the plot (supplemental data). DVR parametric images based on reference Logan were obtained for visualization using wavelet-aided parametric imaging (22). Using cerebellum as reference region, the simplified reference tissue model (SRTM) was also applied (23).

### Late Time (Quasi-Steady-State) Ratio

The time–activity curves for previously developed amyloid- $\beta$  radioligands such as  $^{11}\text{C}$ -PIB have been expressed using standardized uptake values where the target ROIs are corrected for amount of injected activity and body weight. The standard way to quantify amyloid- $\beta$  ligands has then been to calculate standardized uptake value ratios (SUVRs) by dividing the target region by the reference region (cerebellum). SUVr can be viewed as a simplified way to

estimate DVR as has been described elsewhere (24), and the use of a late ratio has often been referred to as the quasi-steady-state approach. We applied this method to calculate SUVRs for  $^{18}\text{F}$ -AZD4694 using data from 51 to 63 min after injection (late ratio).

### Peak Equilibrium Ratio

For neuroreceptor ligands with rapid kinetics, DVR is usually defined using reference Logan or SRTM as described above. In a preliminary attempt to examine another simplified ratio method we calculated SUVRs for  $^{18}\text{F}$ -AZD4694 using an early time interval. Taking advantage of the rapid kinetics of  $^{18}\text{F}$ -AZD4694, the interval was between 21 and 33 min, thereby including the time of the so-called peak equilibrium (peak ratio) (25).

### Test-Retest Reproducibility

For subjects with repeated PET measurements, the test–retest variability was calculated as shown in Equation 1.

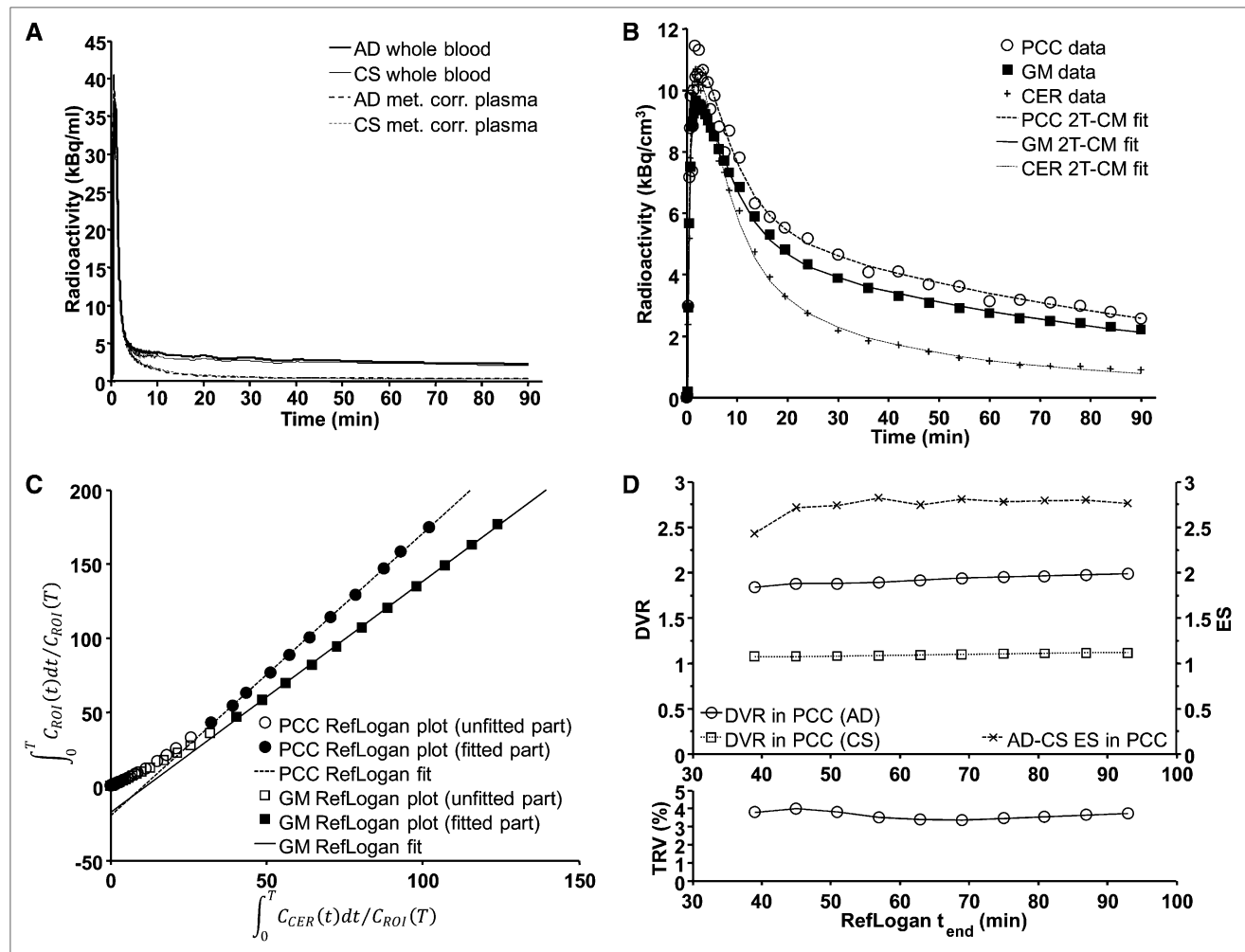


**FIGURE 1.** (A) Mean of radioactivity concentration of  $^{18}\text{F}$ -AZD4694 in arterial whole blood and metabolite-corrected plasma for AD patients ( $n = 10$ ) and CSs ( $n = 6$ ). (B) Two-tissue-compartment model fit to time–activity curves for selected regions of AD patient (AD4). Measured time–activity curves are shown using unconnected markers for posterior cingulate cortex, total gray matter, and cerebellum. Continuous lines represent fitted model curves. (C) Linear graphical analysis using reference Logan: mean plot for AD patients. (D) Demonstration of stability of reference Logan with start time fixed at 27 min after injection and alternating end time. Stability is characterized by showing groupwise interindividual mean of DVR estimates in posterior cingulate cortex, DVR effect size between AD patients ( $n = 10$ ) and CSs ( $n = 6$ ) in posterior cingulate cortex, and test–retest variability in gray matter. CER = cerebellum; ES = effect size; GM = gray matter; PCC = posterior cingulate cortex.

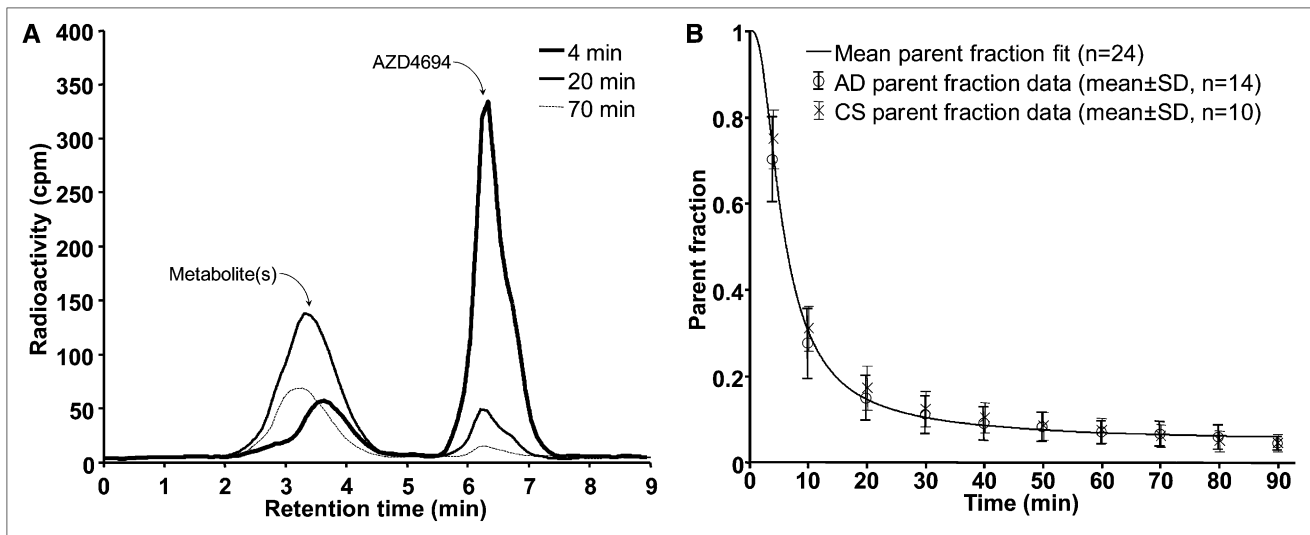


**FIGURE 2.** (A) Chromatogram showing radioactive parent and metabolites of  $^{18}\text{F}$ -AZD4694. (B) Parent fraction of  $^{18}\text{F}$ -AZD4694 vs. time in arterial plasma. Single  $\circ$  and  $\times$  symbols with whiskers indicate groupwise interindividual mean of measured parent fraction data for AD patients ( $n = 10$ ) and CSs ( $n = 6$ ), respectively. Solid line indicates mean of individually fitted parent fraction functions for all subjects.

$$\text{Test-retest variability (\%)} = \frac{|\text{PET}_2 - \text{PET}_1|}{\frac{1}{2}(\text{PET}_1 + \text{PET}_2)} \times 100 \quad \text{Eq. 1}$$

Test-retest variability is reported for selected ROIs as mean  $\pm$  SD across all evaluable subjects.

### Statistical Analysis

Group differences in demographic parameters were assessed using a 2-tailed  $t$  test with unequal variance. The Akaike information criterion was used as an outcome measure to compare the goodness of fit for each compartment and nonlinear model (26). Models were further compared using  $F$  statistics.

The intraclass correlation coefficient was calculated to assess test-retest reliability (27). Group differences in binding parameters were assessed by calculating the standardized difference in group mean estimates between AD patients and CSs. Standardization was based either on the pooled SD producing effect size or on the SD of the control group producing  $z$  scores.

## RESULTS

### Subjects

Six CSs (all men) and 10 AD patients (7 men and 3 women) underwent PET examination according to the protocol. The mean age was  $51 \pm 2$  y in the CSs and  $62 \pm 7$  y in the AD patients ( $P < 0.001$ ). The mean Mini-Mental State Examination score was  $30 \pm 1$  in CSs and  $22 \pm 4$  in AD patients ( $P < 0.001$ ). There was no significant difference in body weight between CSs ( $85 \pm 6$  kg) and AD patients ( $80 \pm 9$  kg) ( $P > 0.05$ ).

### Arterial Input Function and Radioligand Metabolism

The time curves for radioactivity in whole blood and metabolite-corrected plasma were comparable between CSs and AD patients (Fig. 1A). The metabolism of  $^{18}\text{F}$ -AZD4694 was rapid both in CSs and in AD patients. All radioactive metabolites were more polar than the parent compound (Fig. 2A). Approximately 50% of  $^{18}\text{F}$ -AZD4694

was metabolized within 8–9 min after intravenous injection, and about 10% remained unchanged at the end of measurement (Fig. 2B). In both groups, the mean of the ratios between whole brain and metabolite-corrected plasma radioactivity reached an essentially horizontal level during the second half of the measurement (Supplemental Fig. 2).

### Visual Inspection of $^{18}\text{F}$ -AZD4694 Binding

PET images for the peak ratio and late ratio methods and DVR parametric images showed a difference between AD patients and CSs, with higher binding in AD patients throughout most of the cerebral cortex as well as the striatum (Fig. 3). White matter binding was visually low in subcortical regions, especially in the peak ratio SUVR and DVR images.

### Time-Activity Curves

The time-activity curve in whole brain increased rapidly, reaching a peak after about 90 s, when approximately 4% of radioactivity was in the brain (Supplemental Fig. 1). Regional time-activity curves from a representative CS and AD patient are shown in Figure 4. After the initial peak, cortical time-activity curves declined rapidly (Fig. 4). For CSs, the time-activity curves did not differ between target regions and cerebellum (Fig. 4A). In AD patients, the time-activity curves for target ROIs were higher than for cerebellum (Fig. 4B). The time-activity curves for white matter were similar between the subject groups. Compared with cerebellum, the initial peak was lower and then the decline of radioactivity was slower in white matter. White matter values surpassed those for cerebellum from approximately 20 min after injection.

### Compartment Modeling

The regional time-activity curves could be described by the 2-tissue-compartment model (Fig. 1B) but not by

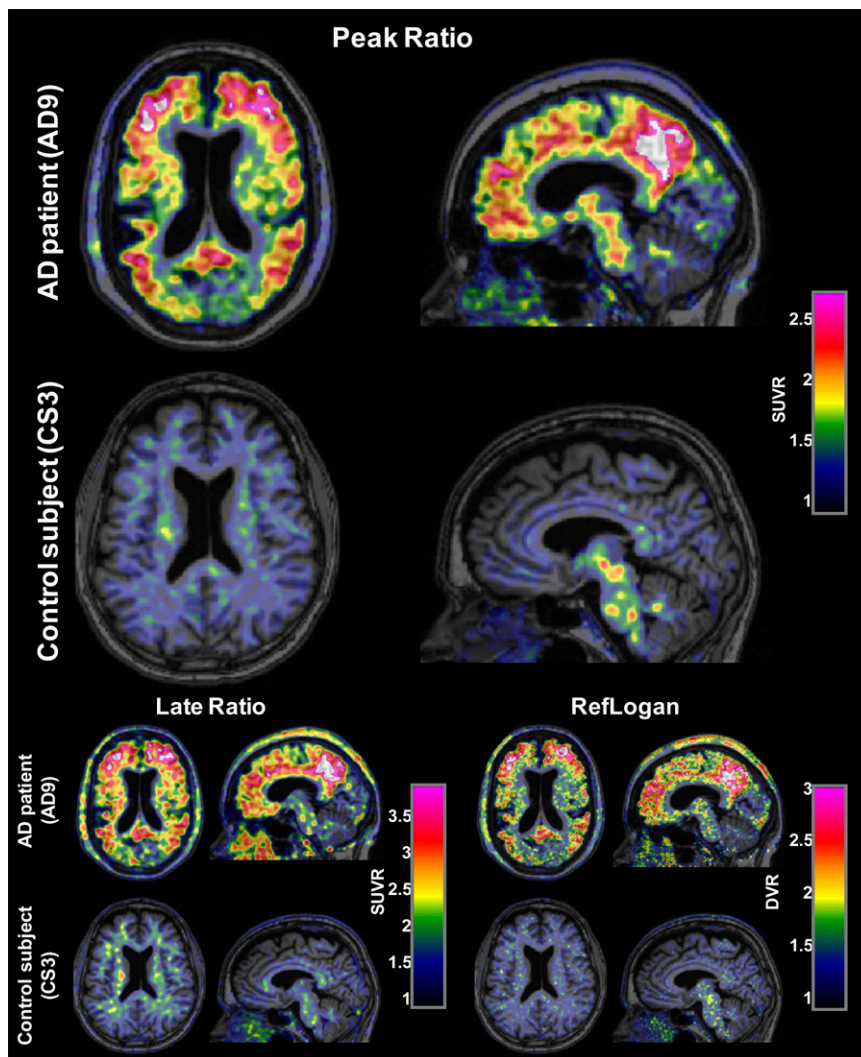


**FIGURE 3.** Sample horizontal and sagittal slices of  $^{18}\text{F}$ -AZD4694 peak ratio (21–33 min), late ratio (51–63 min) SUVR, and reference Logan DVR images overlaid on MR images for AD patient and CS. SUVR images were smoothed for visualization with gaussian filter with full width at half maximum of 5 mm. Color scale windows were set in such a way that cortical binding in AD patient appears comparable between methods.

the 1-tissue-compartment model (Supplemental Fig. 3). The rate constants and derived parameters for the 2-tissue-compartment model are given in Table 1. The supplemental data contain more details.

### Linear Graphical Methods

The Logan and reference Logan plots became linear at a point corresponding to approximately 30 min after injection of  $^{18}\text{F}$ -AZD4694 (Fig. 1C) and produced reliable estimates independent of varying end time or start time (Fig. 1D and Supplemental Fig. 5). Individual reference Logan DVRs are shown in Figure 5. For SRTM, the regional time–activity curves could be described by SRTM (Supplemental Fig. 4). All regional mean DVRs are given in Tables 2 and 3.

### Late Time Ratio Analysis

The ratio between radioactivity in target ROI and reference region in AD patients became stable after approximately 50 min (Fig. 6B). The ratio for gray matter in CSs was close to 1 (Fig. 6B). The calculated SUVRs in AD patients varied between 2.10 and 2.88 across regions (Table 3).

### Peak Equilibrium Analysis

The time–activity curve for specific binding was calculated as the difference between the time–activity curves for a target region and cerebellum. The curve was at peak level between 24 and 30 min after injection and decreased thereafter (Fig. 6A). In CSs, specific binding was negligible (Fig. 6A). Peak ratio SUVRs for AD patients ranged between 1.40 and 2.10 (Table 3).

### Comparisons Between Different Models

Using 2-tissue-compartment model values as the gold standard, the DVRs obtained using reference input (SRTM, reference Logan) were consistent, shown as strong correlations in Table 4. The late ratio approach provided higher SUVRs than any other method, whereas the peak ratio method produced values similar to reference Logan (Tables 2–4).

### Test–Retest Variability

The retest data for AD6 contained severe head-movement artifacts and were thus not suitable for further analysis, leaving 3 AD patients and 4 CSs for test–retest variability assessment.

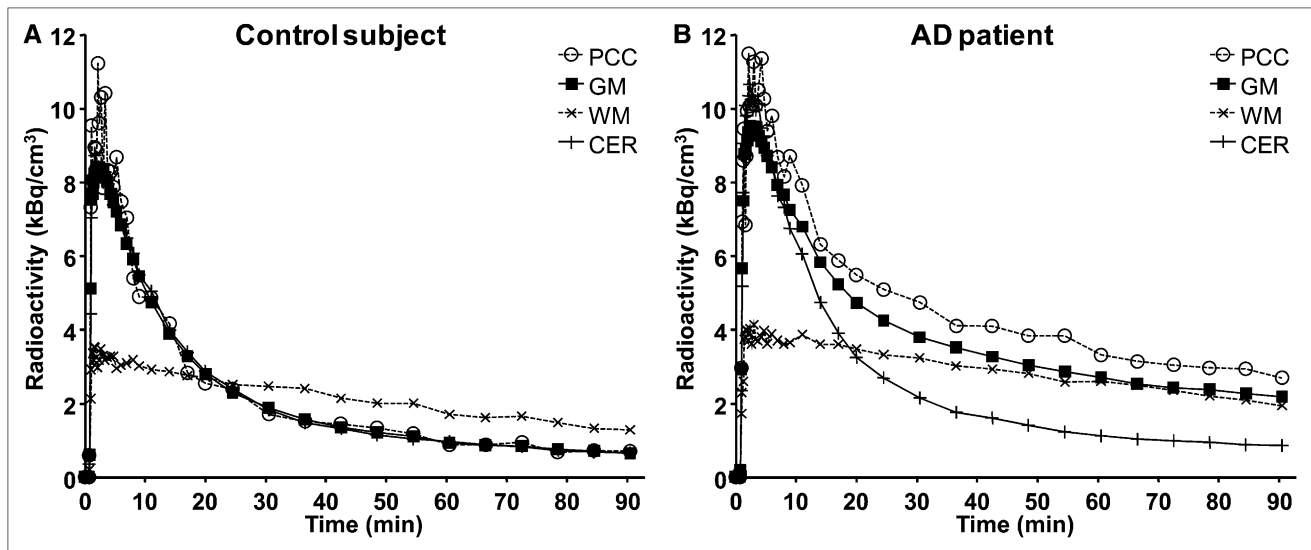


**FIGURE 4.** (A) Regional time-activity curves of CS (A) and AD patient (B). Subject whose time-activity curves were closest to mean time-activity curves in respective group was selected. Selected ROIs are used for illustration. GM = gray matter; CER = cerebellum; PCC = posterior cingulate cortex; WM = white matter.

The test-retest variability for DVR estimates was in the range of 3%–8% in gray matter (Table 5). Intraclass correlation coefficients were generally large, ranging from 0.88 to 0.99 (Table 5).

#### Group Differences in Specific Binding

DVR estimates in CSs were close to 1 for all quantification methods and target regions (Table 2). In contrast, in AD patients most methods provided DVR estimates of around 1.7 for gray matter and close to or greater than 2 in posterior cingulate cortex (Table 3). Individual DVR values with reference Logan even approached 3 (Fig. 5). For all methods, the effect size and  $z$  scores indicated a separation between the 2 groups (Supplemental Table 1). The highest effect sizes and  $z$  scores among methods were obtained using peak ratio for most regions.

#### DISCUSSION

In the present PET study, the kinetic behavior of the novel amyloid- $\beta$  radioligand  $^{18}\text{F}$ -AZD4694 was examined in CSs and probable AD patients.

#### Regional Brain Radioactivity

After intravenous injection of  $^{18}\text{F}$ -AZD4694 in CSs, there were no evident differences in radioactivity between cortical regions and cerebellum. By contrast, in AD patients there was conspicuously higher radioactivity in cortical regions than in cerebellum, a region known to be devoid of substantial amounts of fibrillar A $\beta$  (28). The regional distribution in AD patients had a pattern similar to that shown for other amyloid- $\beta$  PET radioligands (Fig. 3) (2,11,12). Taken together with the previously published detailed autoradiogra-

**TABLE 1**  
Rate Constants and Outcome Estimates Obtained Using 2-Tissue-Compartment Model in Selected Regions

Parameter	CSs ( $n = 6$ )			AD patients ( $n = 10$ )		
	PCC	GM	CER	PCC	GM	CER
$K_1$ (mL/cm $^3$ /min)	0.34 (50%)	0.29 (53%)	0.30 (53%)	0.23 (20%)	0.22 (15%)	0.25 (17%)
$k_2$ (1/min)	0.30 (45%)	0.24 (44%)	0.25 (57%)	0.14 (29%)	0.15 (13%)	0.18 (15%)
$k_3$ (1/min)	0.05 (101%)	0.03 (58%)	0.04 (100%)	0.06 (45%)	0.04 (34%)	0.02 (17%)
$k_4$ (1/min)	0.04 (64%)	0.04 (40%)	0.05 (50%)	0.03 (33%)	0.02 (13%)	0.04 (25%)
$K_1/k_2$	1.20 (27%)	1.19 (16%)	1.21 (11%)	1.75 (26%)	1.51 (20%)	1.42 (23%)
$k_3/k_4$	0.98 (41%)	0.73 (28%)	0.67 (40%)	1.97 (30%)	1.72 (29%)	0.62 (25%)
$V_T$ (mL/cm $^3$ )	2.28 (17%)	2.04 (15%)	1.99 (13%)	5.05 (22%)	4.05 (22%)	2.28 (21%)
DVR	1.14 (14%)	1.02 (7%)	1.00 (0%)	2.26 (23%)	1.81 (21%)	1.00 (0%)
AIC	251 (11%)	156 (28%)	188 (16%)	279 (6%)	161 (14%)	211 (9%)

PCC = posterior cingulate cortex; GM = gray matter; CER = cerebellum;  $V_T$  = total distribution volume; AIC = Akaike information criterion.

Data shown are mean and coefficient of variation.

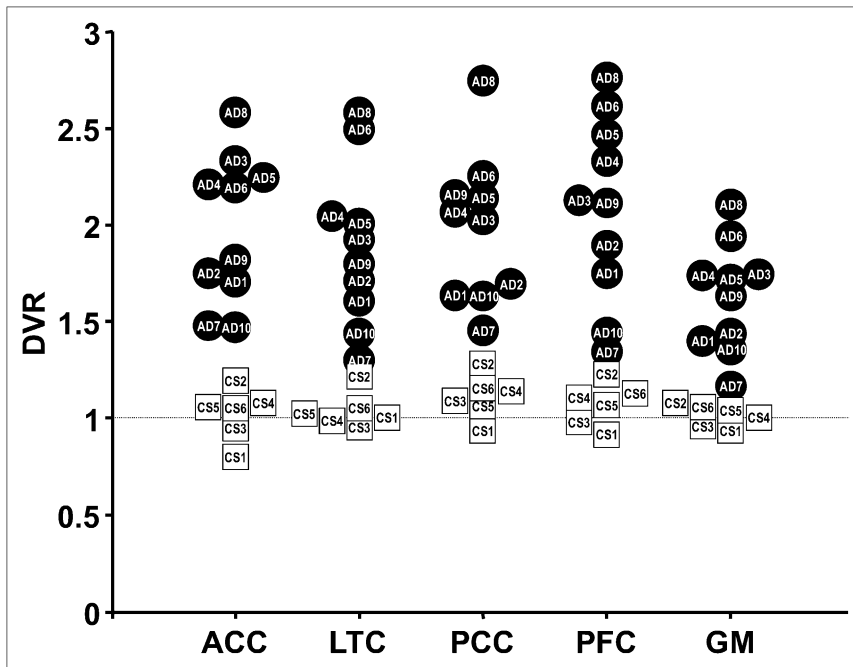


**FIGURE 5.** Scatterplot of individual DVRs in 5 selected regions obtained using reference Logan in AD patients (●) and CSs (□). ACC = anterior cingulate cortex; GM = total gray matter; LTC = lateral temporal cortex; PCC = posterior cingulate cortex; PFC = prefrontal cortex.

phy study of  $^3\text{H}$ -AZD4694 binding in vitro (13), the present observations in vivo support the evidence that  $^{18}\text{F}$ -AZD4694 binds specifically to amyloid- $\beta$  depositions.

#### Radioligand Metabolism and Brain Exposure

The metabolism of  $^{18}\text{F}$ -AZD4694 was rapid, similar to what has been shown for other amyloid- $\beta$  radioligands (12,29–31). The metabolites were more polar than the parent compound (Fig. 2A). The observation that the ratio of radioactivity in brain to metabolite-corrected plasma was nonincreasing, essentially stable in the latter part of the measurement (Supplemental Fig. 2), indirectly supports the interpretation that there is no formation of radioactive metabolites that would gradually enter the brain.

#### Quantitative Analyses

The 2-tissue-compartment model could be used to describe the time–activity curves in CSs and AD patients and was used as the gold standard in the present cross-validation approach.

The rate constants were in general similar to those reported for  $^{11}\text{C}$ -PIB (29), except that the dissociation constant  $k_4$  was relatively high, indicating more rapid dissociation of  $^{18}\text{F}$ -AZD4694 binding. Assuming that radioactivity in the cerebellum serves as an estimate for nonspecific binding, time curves for specific binding were calculated by subtracting the activity of the cerebellum from that of the target region. Specific binding peaked at about 27 min after injection and declined thereafter. Such observations have in

**TABLE 2**  
DVR and SUVR Obtained in All Quantification Methods and Regions in CSs

ROI	DVR					SUVR	
	1T-CM	2T-CM	Logan	SRTM	Reference Logan	Peak ratio (21–33)	Late ratio (51–63)
Anterior cingulate cortex	1.02 (13%)	1.05 (16%)	1.02 (17%)	1.02 (18%)	1.02 (13%)	1.06 (10%)	1.12 (29%)
Lateral temporal cortex	1.04 (9%)	1.06 (11%)	1.05 (11%)	1.05 (11%)	1.04 (9%)	1.04 (8%)	1.12 (15%)
Parietal cortex	1.06 (6%)	1.11 (9%)	1.10 (9%)	1.14 (14%)	1.08 (7%)	1.05 (5%)	1.16 (13%)
Posterior cingulate cortex	1.08 (11%)	1.14 (14%)	1.15 (14%)	1.21 (23%)	1.11 (10%)	1.08 (12%)	1.23 (16%)
Prefrontal cortex	1.06 (10%)	1.10 (13%)	1.09 (14%)	1.10 (17%)	1.07 (10%)	1.06 (8%)	1.15 (19%)
White matter	1.45 (22%)	1.51 (23%)	1.42 (24%)	1.38 (20%)	1.31 (19%)	1.30 (14%)	1.94 (29%)
Gray matter	1.00 (5%)	1.02 (7%)	1.02 (8%)	1.05 (10%)	1.01 (6%)	1.01 (5%)	1.08 (11%)
Cerebellum ( $V_T$ )	1.89 (14%)	1.99 (13%)	2.05 (14%)	—	—	—	—

1T-CM = 1-tissue-compartment model; 2T-CM = 2-tissue-compartment model;  $V_T$  = total distribution volume. Data are mean and coefficient of variation ( $n = 6$ ).

**TABLE 3**  
DVR and SUVR Obtained in All Quantification Methods and Regions in AD Patients

ROI	DVR					SUVR	
	1T-CM	2T-CM	Logan	SRTM	Reference Logan	Peak ratio (21–33)	Late ratio (51–63)
Anterior cingulate cortex	2.20 (23%)	2.31 (23%)	2.20 (23%)	2.05 (19%)	1.98 (19%)	1.97 (20%)	2.75 (24%)
Lateral temporal cortex	2.09 (26%)	2.22 (26%)	2.12 (26%)	1.92 (22%)	1.89 (22%)	1.90 (19%)	2.59 (28%)
Parietal cortex	2.17 (26%)	2.29 (25%)	2.20 (26%)	2.01 (23%)	1.96 (22%)	1.99 (23%)	2.71 (27%)
Posterior cingulate cortex	2.19 (23%)	2.26 (23%)	2.16 (24%)	2.05 (21%)	1.98 (19%)	2.05 (18%)	2.73 (25%)
Prefrontal cortex	2.30 (26%)	2.40 (26%)	2.33 (27%)	2.15 (24%)	2.08 (23%)	2.10 (21%)	2.88 (30%)
White matter	1.67 (19%)	1.61 (21%)	1.50 (22%)	1.44 (17%)	1.39 (18%)	1.40 (18%)	2.10 (21%)
Gray matter	1.73 (21%)	1.81 (21%)	1.78 (21%)	1.68 (18%)	1.62 (18%)	1.65 (17%)	2.15 (24%)
Cerebellum ( $V_T$ )	2.02 (23%)	2.28 (21%)	2.34 (21%)	—	—	—	—

1T-CM = 1-tissue-compartment model; 2T-CM = 2-tissue-compartment model;  $V_T$  = total distribution volume. Data shown are mean and coefficient of variation ( $n = 10$ ).

the literature been referred to as peak equilibrium (8). Besides providing additional support for the reversible nature of  $^{18}\text{F}$ -AZD4694 binding, the rapidly peaking kinetics allow for application of simplified quantitative approaches previously developed for reversible neuroreceptor radioligands (8,20,23,32).

Furthermore, the time–activity curves for white matter differed from other regions and showed a lower initial peak and a slower decline rendering a relatively high level during the latter part of the PET acquisition. Such presence of relatively high nonspecific binding in white matter has been observed also for other amyloid- $\beta$  radioligands (11,12,31). The potential for quantification at a time when binding in white matter is still relatively low was a further reason for implementing a preliminary peak ratio approach.

### Quantitative Methods of Choice

The estimates obtained with the simplified methods correlated with the 2-tissue-compartment model (Table 4). Reference tissue approaches such as reference Logan and SRTM underestimated the DVR, as has been observed also for  $^{11}\text{C}$ -PIB (33) and some receptor radioligands (34), whereas the late ratio approach overestimated amyloid- $\beta$  binding as compared with the 2-tissue-compartment model. This overestimation is a common observation for receptor radioligands such as  $^{18}\text{F}$ -cyclofoxy (35), and the theoretic underpinnings have been further examined in detail in a PET study using the  $\text{D}_2$ -dopamine receptor radioligand  $^{11}\text{C}$ -FLB 457 ((*S*)-*N*-((1-ethyl-2-pyrrolidinyl)methyl)-5-bromo-2,3-dimethoxybenzamide) (36). Importantly, the peak ratio and reference Logan methods provided similar estimates that correlated well with

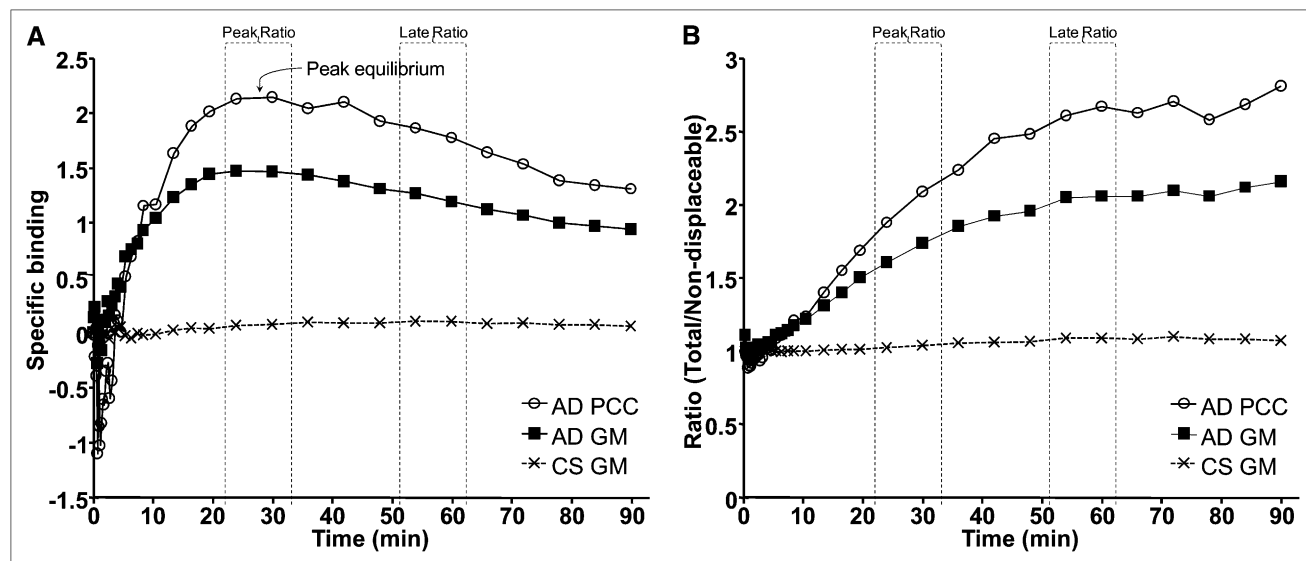


**FIGURE 6.** (A) Groupwise interindividual mean of specific binding vs. time for selected regions in AD patients ( $n = 10$ ) and CSs ( $n = 6$ ). (B) Groupwise interindividual mean of ratio of time–activity curves of selected target regions and cerebellum vs. time in AD patients and CSs. GM = gray matter; PCC = posterior cingulate cortex.

**TABLE 4**  
Correlation and Regression Between 2T-CM and Other Means of Quantification

2T-CM vs.:	<i>R</i>	<i>P</i>	Line equation*
1T-CM	0.98	$2.7 \times 10^{-118}$	$0.93x + 0.05$
Logan	1.00	$2.2 \times 10^{-195}$	$0.95x + 0.04$
SRTM	0.98	$6.2 \times 10^{-109}$	$0.80x + 0.22$
Reference Logan	1.00	$3.0 \times 10^{-161}$	$0.76x + 0.24$
Peak ratio (21–33)	0.97	$3.9 \times 10^{-95}$	$0.75x + 0.29$
Late ratio (51–63)	0.99	$6.3 \times 10^{-125}$	$1.30x - 0.26$

\*Slope and intercept of regression line.

1T-CM = 1-tissue-compartment model; 2T-CM = 2-tissue-compartment model.

Correlation is based on all individual regional estimates, excluding cerebellum, in all subjects ( $n = 16$ ).

those from the 2-tissue-compartment model, and the methods may thus be viewed as validated for quantification.

<sup>18</sup>F-AZD4694 has several favorable properties for use in a clinical setting. Arterial blood sampling is not required for quantitation, since methods using a reference input provided valid estimates of amyloid- $\beta$  load. The reference Logan analyses also showed that using 45 min of acquisition data provides reliable DVRs (Fig. 1D), supporting the possibility that a short acquisition might be sufficient to quantify amyloid- $\beta$  load. The advantages of the peak ratio method include short data acquisition and simple practical use. However, this method requires further examination regarding sensitivity to the timing of acquisition and optimal time interval for reliable analysis. The fact that <sup>18</sup>F-AZD4694 has potential to be shipped to hospitals without an in-house cyclotron and radiochemistry further increases the potential for wide use in clinical settings.

#### Test–Retest Analysis

Good reliability is important when studying longitudinal changes of amyloid- $\beta$  load in the course of the disease or during disease-modifying therapy. The preliminary test–retest analysis provided mean differences ranging between

3% and 11% depending on region and quantitative approach (Table 5). The lowest variability among noninvasive methods was obtained for the reference Logan approach. However, the test–retest reproducibility needs to be further examined in a larger sample before a clear judgment of reliability can be made.

#### Limitations

The analysis did not include correction for partial-volume effect. However, the images were obtained with a high-resolution research tomograph having an effective resolution of 1.5 mm (full width at half maximum) and thus less need to correct for partial-volume effect. In addition, omitting this correction is the more conservative approach when evaluating a new radioligand for amyloid- $\beta$  imaging (37,38).

#### Comparison with Other Amyloid- $\beta$ Radioligands

The rapid binding kinetics of <sup>18</sup>F-AZD4694 may differentiate it from other amyloid- $\beta$  radioligands, such as <sup>11</sup>C-PIB, which show slower kinetics with a blunt peak of specific binding followed by a slower decline (based on time–activity curves (7,29)). However, detailed comparison between <sup>18</sup>F-AZD4694 and published data for other <sup>18</sup>F-radioligands targeting amyloid- $\beta$  is hampered by differences in PET resolution, evaluation methods such as delineation of ROIs, and means of quantification. Future head-to-head comparisons between <sup>18</sup>F-AZD4694 and other amyloid- $\beta$  radioligands are thus strongly required.

#### CONCLUSION

The binding of the novel radioligand <sup>18</sup>F-AZD4694 to amyloid- $\beta$  deposits in AD brains has a regional distribution in concordance with previous preclinical analyses and other amyloid- $\beta$  radioligands. The time–activity curves could be adequately described using traditional arterial input–based compartment modeling, which also was applied to validate the use of simplified methods. The rapid specific binding kinetics allow for quantification using data based on short acquisitions. Valid estimates of amyloid- $\beta$  binding could be obtained using the cerebellum as a reference region in

**TABLE 5**  
Data Based on Results in All Evaluable Test–Retest Subjects ( $n = 7$ )

Model	Parameter	Total gray matter		Posterior cingulate cortex	
		TRV (%)	ICC	TRV (%)	ICC
1 tissue compartment	DVR	$3.8 \pm 1.5$	0.99	$6.4 \pm 3.7$	0.98
2 tissue compartments	DVR	$3.1 \pm 2.4$	0.99	$6.9 \pm 5.5$	0.96
Logan	DVR	$4.1 \pm 2.8$	0.98	$7.6 \pm 4.9$	0.95
SRTM	DVR	$4.7 \pm 4.5$	0.97	$11.2 \pm 7.9$	0.88
Reference Logan	DVR	$3.7 \pm 1.9$	0.98	$5.8 \pm 4.3$	0.96
Peak ratio (21–33)	SUVr	$6.0 \pm 3.4$	0.96	$10.2 \pm 5.9$	0.97
Late ratio (51–63)	SUVr	$7.5 \pm 6.5$	0.95	$7.8 \pm 5.3$	0.97

Data are mean  $\pm$  SD for test–retest variability (TRV) and intraclass correlation coefficient (ICC).

approaches such as reference Logan. Simple quantification together with the fact that  $^{18}\text{F}$ -AZD4694 is labeled with  $^{18}\text{F}$  constitutes 2 cornerstones for wider use in clinical settings.

## DISCLOSURE STATEMENT

The costs of publication of this article were defrayed in part by the payment of page charges. Therefore, and solely to indicate this fact, this article is hereby marked “advertisement” in accordance with 18 USC section 1734.

## ACKNOWLEDGMENTS

We thank the patients, their relatives, and the healthy volunteers who participated in this study. We gratefully acknowledge the efforts and support by all members of the Karolinska Institutet PET group. We thank Britt Marie Swahn for dedicated medicinal chemistry support in radioligand development and Ulrika Lönnqvist-Akenine for excellent patient management. No potential conflict of interest relevant to this article was reported.

## REFERENCES

1. Ikonovic MD, Klunk W, Abrahamson E, et al. Post-mortem correlates of in vivo PiB-PET amyloid imaging in a typical case of Alzheimer's disease. *Brain*. 2008;131:1630–1645.
2. Klunk WE, Engler H, Nordberg A, et al. Imaging brain amyloid in Alzheimer's disease with Pittsburgh Compound-B. *Ann Neurol*. 2004;55:306–319.
3. Forsberg A, Engler H, Almkvist O, et al. PET imaging of amyloid deposition in patients with mild cognitive impairment. *Neurobiol Aging*. 2008;29:1456–1465.
4. Villemagne VL, Pike KE, Chételat G, et al. Longitudinal assessment of A $\beta$  and cognition in aging and Alzheimer disease. *Ann Neurol*. 2011;69:181–192.
5. Rinne JO, Brooks D, Rossor M, et al.  $^{11}\text{C}$ -PiB PET assessment of change in fibrillar amyloid-beta load in patients with Alzheimer's disease treated with bapineuzumab: a phase 2, double-blind, placebo-controlled, ascending-dose study. *Lancet Neurol*. 2010;9:363–372.
6. Blomquist G, Engler H, Nordberg A, et al. Unidirectional influx and net accumulation of PiB. *Open Neuroimag J*. 2008;2:114–125.
7. Lopresti BJ, Klunk W, Mathis C, et al. Simplified quantification of Pittsburgh compound B amyloid imaging PET studies: a comparative analysis. *J Nucl Med*. 2005;46:1959–1972.
8. Farde L, Eriksson L, Blomquist G, Halldin C. Kinetic analysis of central [ $^{11}\text{C}$ ]raclopride binding to D2-dopamine receptors studied by PET: a comparison to the equilibrium analysis. *J Cereb Blood Flow Metab*. 1989;9:696–708.
9. Vandenbergh R, Van Laere K, Ivanou A, et al.  $^{18}\text{F}$ -flutemetamol amyloid imaging in Alzheimer disease and mild cognitive impairment: a phase 2 trial. *Ann Neurol*. 2010;68:319–329.
10. Clark CM, Schneider JA, Bedell BJ, et al. Use of florbetapir-PET for imaging beta-amyloid pathology. *JAMA*. 2011;305:275–283.
11. Barthel H, Luthardt J, Becker G, et al. Individualized quantification of brain  $\beta$ -amyloid burden: results of a proof of mechanism phase 0 florbetaben PET trial in patients with Alzheimer's disease and healthy controls. *Eur J Nucl Med Mol Imaging*. 2011;38:1702–1714.
12. Nelissen N, Van Laere K, Thurfjell L, et al. Phase 1 study of the Pittsburgh compound B derivative  $^{18}\text{F}$ -flutemetamol in healthy volunteers and patients with probable Alzheimer disease. *J Nucl Med*. 2009;50:1251–1259.
13. Juréus A, Swahn BM, Sandell J, et al. Characterization of AZD4694, a novel fluorinated Abeta plaque neuroimaging PET radioligand. *J Neurochem*. 2010;114:784–794.
14. Allen F. *Diagnostic and Statistical Manual of Mental Disorders: DSM-IV*. Washington, DC: American Psychiatric Association; 1994.
15. Varrone A, Sjöholm N, Eriksson L, Gulyás B, Halldin C, Farde L. Advancement in PET quantitation using 3D-OP-OSEM point spread function reconstruction with the HRRT. *Eur J Nucl Med Mol Imaging*. 2009;36:1639–1650.
16. Halldin C, Farde L, Höglberg T, et al. Carbon-11-FLB 457: a radioligand for extrastriatal D2 dopamine receptors. *J Nucl Med*. 1995;36:1275–1281.
17. Roland PE, Zilles K. Brain atlases: a new research tool. *Trends Neurosci*. 1994;17:458–467.
18. Svarer C, Madsen K, Hasselbalch SG, et al. MR-based automatic delineation of volumes of interest in human brain PET images using probability maps. *Neuroimage*. 2005;24:969–979.
19. Cselényi Z, Olsson H, Halldin C, Gulyás B, Farde L. A comparison of recent parametric neuroreceptor mapping approaches based on measurements with the high affinity PET radioligands [ $^{11}\text{C}$ ]FLB 457 and [ $^{11}\text{C}$ ]WAY 100635. *Neuroimage*. 2006;32:1690–1708.
20. Logan J, Fowler JS, Volkow ND, et al. Graphical analysis of reversible radioligand binding from time-activity measurements applied to [ $^{11}\text{C}$ -methyl]-(-)-cocaine PET studies in human subjects. *J Cereb Blood Flow Metab*. 1990;10:740–747.
21. Logan J, Fowler JS, Volkow ND, Wang GJ, Ding YS, Alexoff DL. Distribution volume ratios without blood sampling from graphical analysis of PET data. *J Cereb Blood Flow Metab*. 1996;16:834–840.
22. Cselényi Z, Olsson H, Farde L, Gulyás B. Wavelet-aided parametric mapping of cerebral dopamine D2 receptors using the high affinity PET radioligand [ $^{11}\text{C}$ ]FLB 457. *Neuroimage*. 2002;17:47–60.
23. Lammertsma AA, Hume SP. Simplified reference tissue model for PET receptor studies. *Neuroimage*. 1996;4:153–158.
24. Thie JA. Understanding the standardized uptake value, its methods, and implications for usage. *J Nucl Med*. 2004;45:1431–1434.
25. Olsson H, Halldin C, Swahn CG, Farde L. Quantification of [ $^{11}\text{C}$ ]FLB 457 binding to extrastriatal dopamine receptors in the human brain. *J Cereb Blood Flow Metab*. 1999;19:1164–1173.
26. Akaike H. A new look at statistical model identification. *IEEE Trans Automatic Control*. 1974;19:716–723.
27. Shrout PE, Fleiss JL. Intra-class correlations: uses in assessing rater reliability. *Psychol Bull*. 1979;86:420–428.
28. Svedberg M, Hall H, Hellström-Lindahl E, et al. [ $^{11}\text{C}$ ]PiB-amyloid binding and levels of Abeta40 and Abeta42 in postmortem brain tissue from Alzheimer patients. *Neurochem Int*. 2009;54:347–357.
29. Price JC, Klunk W, Lopresti B, et al. Kinetic modeling of amyloid binding in humans using PET imaging and Pittsburgh compound-B. *J Cereb Blood Flow Metab*. 2005;25:1528–1547.
30. Rowe CC, Ackerman U, Browne W, et al. Imaging of amyloid beta in Alzheimer's disease with  $^{18}\text{F}$ -BAY94-9172, a novel PET tracer: proof of mechanism. *Lancet Neurol*. 2008;7:129–135.
31. Wong DF, Rosenberg PB, Zhou Y, et al. In vivo imaging of amyloid deposition in Alzheimer disease using the radioligand  $^{18}\text{F}$ -AV-45 (florbetapir F 18). *J Nucl Med*. 2010;51:913–920.
32. Farde L, Ito H, Swahn CG, Pike VW, Halldin C. Quantitative analyses of carbonyl-carbon-11-WAY-100635 binding to central 5-hydroxytryptamine-1A receptors in man. *J Nucl Med*. 1998;39:1965–1971.
33. Yaquob M, Tolboom N, Boellaard R, et al. Simplified parametric methods for [ $^{11}\text{C}$ ]PiB studies. *Neuroimage*. 2008;42:76–86.
34. Gunn RN, Lammertsma AA, Hume SP, Cunningham VJ. Parametric imaging of ligand-receptor binding in PET using a simplified reference region model. *Neuroimage*. 1997;6:279–287.
35. Carson RE, Channing MA, Blasberg RG, et al. Comparison of bolus and infusion methods for receptor quantitation: application to [ $^{18}\text{F}$ ]cyclofoxy and positron emission tomography. *J Cereb Blood Flow Metab*. 1993;13:24–42.
36. Olsson H, Farde L. Potentials and pitfalls using high affinity radioligands in PET and SPET determinations on regional drug induced D2 receptor occupancy: a simulation study based on experimental data. *Neuroimage*. 2001;14:936–945.
37. Drzezga A, Grimmer T, Henriksen G, et al. Effect of APOE genotype on amyloid plaque load and gray matter volume in Alzheimer disease. *Neurology*. 2009;72:1487–1494.
38. Bourgeat P, Chételat G, Villemagne V, et al. Beta-amyloid burden in the temporal neocortex is related to hippocampal atrophy in elderly subjects without dementia. *Neurology*. 2010;74:121–127.